Covalent Titanium Aryldioxy One-, Two-, and Three-Dimensional Networks and Their Examination as Ziegler−Natta Catalysts

Joseph M. Tanski and Peter T. Wolczanski*

Department of Chemistry and Chemical Biology, Baker Laboratory, Cornell University, Ithaca, New York 14853

Received July 11, 2000

Treatment of $(^{i}PrO)_4Ti$ with 2,7-dihydroxynaphthalene at 100 °C afforded the one-dimensional ladder [*cis*-Ti($\mu_{2,7}$-$OC_{10}H_6O)_2py_2]_n$ (**1**: $C_{30}H_{22}N_2O_4Ti$, orthorhombic, $P2_12_12_1$, $a = 9.866(2)$ Å, $b = 15.962(3)$ Å, $c = 16.223(3)$ Å, $Z = 4$), in pyridine, and the stacked ladder, two-dimensional [Ti($\mu_{2,7}$-$OC_{10}H_6O)_2$(4-picoline)$_2$·(4-picoline)$_{0.5}]_n$ (**2**: $C_{70}H_{59}N_5O_8Ti_2$, triclinic, $P\bar{1}$, $a = 10.814(2)$ Å, $b = 16.785(3)$ Å, $c = 18.020(4)$ Å, $\alpha = 93.88(3)°$, $\beta = 107.31(3)°$, $\gamma = 108.77(3)°$, $Z = 2$), in 4-picoline. A disruption of intramolecular edge-to-face and intermolecular face-to-face π-stacking interactions in **1** by the Me group of the 4-picoline causes the structural change to **2**. These derivatives and related two- and three-dimensional covalent metal organic networks (CMON) were assayed for ethylene and propylene polymerization activity via the addition of methylaluminoxane. CMON are mediocre Ziegler−Natta catalysts that generate polydisperse, linear polyethylene and atactic polypropylene. The data are best accommodated by viewing the degradation of CMON into numerous active sites of differing activity.

Introduction

Since the discovery of Ziegler−Natta (ZN) olefin polymerization catalysts in the 1950s, polyolefin production has been of major industrial importance. Recently, the discovery of metallocene and related single-site homogeneous catalysts that permit greater control of the density and stereochemistry of polyolefins has rejuvenated the field and changed the character of the marketplace for these products.[1−7] Despite such landmark advances in homogeneous catalysis, a significant fraction of polyolefins are made via heterogeneous methods. Furthermore, supported catalysts that combine the selectivity of homogeneous materials and the ready processing advantages of heterogeneous catalysts are in great demand.[6,7] The classic example of a heterogeneous Ziegler−Natta catalyst is $TiCl_3$ supported on $MgCl_2$, which is used to produce isotactic polypropylene.[3] While the site symmetry and mechanism of this stereoselective polymerization are still subject to some debate, one aspect of this type of catalyst is clear: in contrast to homogeneous catalysts, the use of metal halides as either the reactive center or support does not permit much structural diversity. Given the resurgence in the coordination polymerization of transition metals,[8−10] an investigation of these materials as ZN catalysts, especially considering their scope, is clearly prudent. Current methodologies may allow the syntheses of heterogeneous materials that act as single-site catalysts.[6,7,10]

Covalent metal−organic networks (CMON)[11−16] synthesized from early transition metals, aryldioxide organic spacers, and simple donor ligands are a class of compounds readily assessed for polymerization activity. Thus far, two- and three-dimensional CMON derivatives of titanium exist and representatives are illustrated in Figure 1. CMON species of the type [*cis*- or *trans*-(μ-OArO)$_4$Ti(py)$_2]_n$,[14] where OArO stands for an aryldioxide

(1) Coates, G. W. *Chem. Rev.* **2000**, *100*, 1223−1252.
(2) Brintzinger, H. H.; Fischer, D.; Mülhaupt, R.; Rieger, B.; Waymouth, R. M. *Angew. Chem., Int. Ed. Engl.* **1995**, *34*, 1143−1170.
(3) Resconi, L.; Cavallo, L.; Fait, A.; Piemontesi, F. *Chem. Rev.* **2000**, *100*, 1253−1346.
(4) Alt, H. G.; Köppl, A. *Chem. Rev.* **2000**, *100*, 1205−1222.
(5) Kaminsky, W.; Arndt, M. *Adv. Polym. Sci.* **1997**, *127*, 143−187.
(6) Hlatky, G. G. *Chem. Rev.* **2000**, *100*, 1347−1376.
(7) Fink, G.; Steinmetz, B.; Zechlin, J.; Przybyla, C.; Tesche, B. *Chem. Rev.* **2000**, *100*, 1377−1390.
(8) (a) O'Keeffe, M.; Eddaoudi, M.; Li, H.; Reineke, T.; Yaghi, O. M. *J. Solid State Chem.* **2000**, *152*, 3−20. (b) Batten, S. R.; Robson, R. *Angew. Chem., Int. Ed.* **1998**, *37*, 1460−1494. (c) Janiak, C. *Angew. Chem., Int. Ed. Engl.* **1997**, *36*, 1431−1434. (d) Zaworotko, M. J. *Angew. Chem., Int. Ed.* **1998**, *37*, 1211−1213.
(9) For a sampling of recent, intriguing transition metal coordination polymers, see the following. (a) Barandika, M. G.; Hernandez-Pino, L.; Urtiaga, M. K. Cortes, R.; Lezama, L.; Arriortua, I.; Rojo, T. *J. Chem. Soc., Dalton Trans.* **2000**, 1469−1473. (b) Michelsen, U.; Hunter, C. A. *Angew. Chem., Int. Ed.* **2000**, *39*, 764−767. (c) Pan, L.; Huang, X.; Li, J.; Wu, Y.; Zheng, N. *Angew. Chem., Int. Ed.* **2000**, *39*, 527−530. (d) Montserrat, M.; Resino, I.; Ribas, j.; Stoeckli-Evans, H. *Angew. Chem., Int. Ed.* **2000**, *39*, 191−193. (e) Diskin-Posner, Y.; Dahal, S.; Goldberg, I. *Angew. Chem., Int. Ed.* **2000**, *39*, 1288−1292. (f) Carlucci, L.; Ciani, G.; Moret, M.; Proserpio, D. M.; Rizzato, S. *Angew. Chem., Int. Ed.* **2000**, *39*, 1506−1510. (g) Lightfoot, P.; Snedden, A. J. *J. Chem. Soc., Dalton Trans.* **1999**, 3549−3551. (h) Wang, D.; Yu, R.; Kumada, N.; Kinomura, N. *Chem. Mater.* **1999**, *11*, 2008−2012. (i) Niu, T.; Wang, X.; Jacobson, A. J. *Angew. Chem., Int. Ed.* **1999**, *38*, 1934−1936. (j) Batten, S. R.; Jensen, P.; Moubaraki, B.; Murray, K. S.; Robson, R. *J. Chem. Soc., Chem. Commun.* **1998**, 439−440. (k) Lloret, F.; De Munno, G.; Julve, M.; Cano, J.; Ruiz, R.; Caneschi, A. *Angew. Chem., Int. Ed.* **1998**, *37*, 135−138.
(10) Liu, F.-Q.; Tilley, T. D. *J. Chem. Soc., Chem. Commun.* **1998**, 103−104.
(11) Vaid, T. P.; Lobkovsky, E. B.; Wolczanski, P. T. *J. Am. Chem. Soc.* **1997**, *119*, 874−875.
(12) Vaid, T. P.; Tanski, J. M.; Pette, J. M.; Lobkovsky, E. B.; Wolczanski, P. T. *Inorg. Chem.* **1999**, *38*, 3394−3405.
(13) Tanski, J. M.; Lobkovsky, E. B.; Wolczanski, P. T. *J. Solid State Chem.* **2000**, *152*, 130−140.
(14) Tanski, J. M.; Vaid, T. P.; Lobkovsky, E. B.; Wolczanski, P. T. *Inorg. Chem.* **2000**, *39*, 4756−4765.
(15) Tanski, J. M.; Wolczanski, P. T. *Inorg. Chem.* **2001**, *40*, 346−353. Vanadium CMON species generated via redox reactions are entailed herein.
(16) Tanski, J. M. Ph.D. Thesis, Cornell University, Ithaca, NY, 2000. Only {[Ti($\mu_{2,6}$:η^2,η^1-$OC_{10}C_6O$)($\mu_{2,6}$-$OC_{10}C_6OH)_2]_2$·$C_6H_6\}_n$ manifests a 10-connected network, where redundant $\mu_{2,6}$:η^2,η^1-$OC_{10}C_6O$ linkages connect dititanium centers in an overall body-centered motif.

10.1021/ic000763n CCC: $20.00
Published on Web 03/21/2001

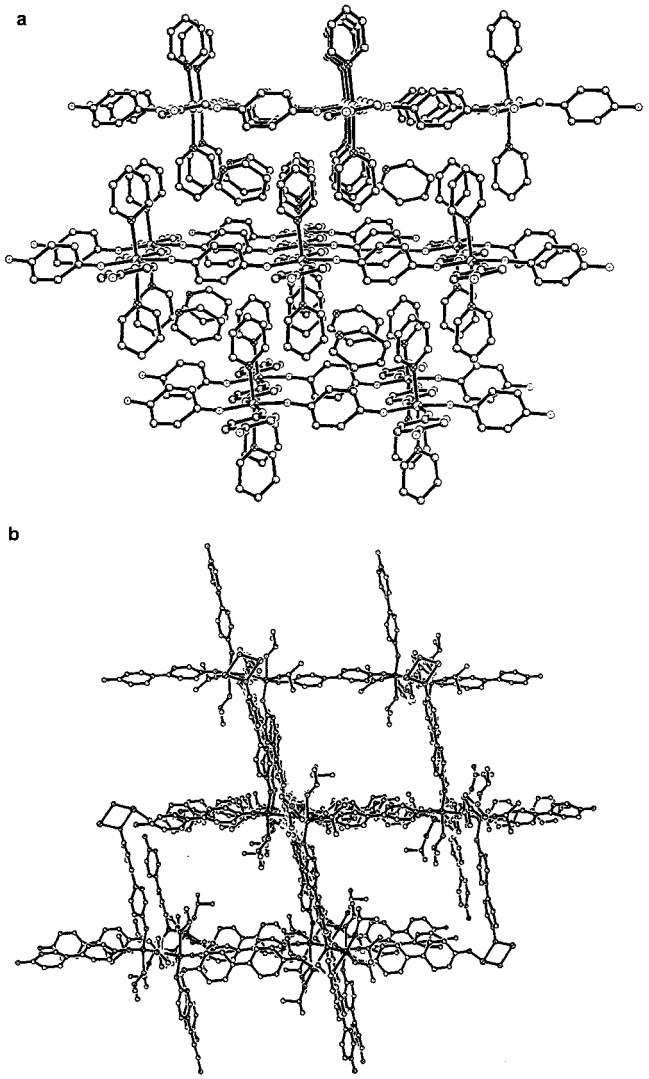

Figure 1. Views of two-dimensional (a) [*trans*-Ti($\mu_{1,4}$-OC_6H_4O)$_2$-py_2.py]$_n$ and (b) {[Ti(μ:η^2,η^1-4,4′-$OC_{12}H_8O$)$_{0.5}$(μ-4,4′-$OC_{12}H_8O$)(O^iPr)-(HO^iPr)]$_2$·THF}$_n$.

ligand capable of spanning at least two metal centers and py is a substituted or unsubstituted pyridine, form sheet or rippled sheet structures, such as that of [*trans*-Ti($\mu_{1,4}$-OC_6H_4O)$_2$$py_2$·py]$_n$ shown. Three-dimensional CMON species typically possess body-centered, hexagonal, or primitive motifs, depending on the connectivity of the bioctahedral, dititanium Ti_2(μ-OArO)$_2$-containing building block intrinsic to each compound. A maximum of 10 connections can be made from the bioctahedron,[16] and 8 are utilized in generating body-centered (e.g., [Ti_2-($\mu_{1,4}$-OC_6H_4O)$_2$($\mu_{1,4}$-OC_6H_4OH)$_2$(μ-OC_6H_4OH)$_2$]$_n$, [Ti_2($\mu_{2,7}$-$OC_{10}H_6O$)$_2$($\mu_{2,7}$:η^2,η^1-$OC_{10}H_6OH$)$_2$(O^iPr)$_2$]$_n$) and hexagonal (e.g., [Ti_2($\mu_{1,4}$-OC_6H_4O)$_2$($\mu_{1,4}$:η^2,η^1-OC_6H_4O)$_2$$(OH_2)_2$·$(H_2O)_2$·(HO−$C_6H_4OH$)·(MeCN)]$_n$) networks.[12] Only six comprise the primitive motif accorded {[Ti(μ:η^2,η^1-4,4′-$OC_{12}H_8O$)$_{0.5}$(μ-4,4′-$OC_{12}H_8O$)(O^iPr)(HO^iPr)]$_2$·THF}$_n$,[13] whose longer spacer and lesser connectivity lead to the larger channels clearly indicated in Figure 1.

In attempting to create CMON derivatives with larger channels, 2,7-dihydroxynaphthalene has been employed[12,15] in synthetic schemes that include pyridine and 4-picoline. Instead of observing two-dimensional materials with large channels, void space is averted by a lowering of CMON dimensionality to form a 1-D ladder compound in pyridine. The subtle change to 4-picoline redirected the CMON to a two-dimensional material but one unlike all previous sheets. With the three different dimensionalities of CMON now available, an assay of Ziegler−Natta catalyst activity of all titanium CMON is presented.

Table 1. Crystallographic Data for [*cis*-Ti($\mu_{2,7}$-$OC_{10}H_6O$)$_2$$(py)_2$]$_n$ (**1**) and [*cis*-Ti($\mu_{2,7}$-$OC_{10}H_6O$)$_2$(4-Me-py)$_2$·(4-Me-py)0.5]$_n$ (**2**)

	1	**2**
formula	$C_{30}H_{22}N_2O_4Ti$	$C_{70}H_{59}N_5O_8Ti_2$
fw	523.40	1194.02
space group	$P2_12_12_1$	$P\bar{1}$
Z	4	2
a, Å	9.866 (2)	10.814 (2)
b, Å	15.962 (3)	16.785 (3)
c, Å	16.223 (3)	18.020 (4)
α, deg	90	93.88 (3)
β, deg	90	107.31 (3)
γ, deg	90	108.77 (3)
V, Å^3	2554.8(9)	2907.8 (10)
ρ_{calc}, g cm^{-3}	1.361	1.364
μ, cm^{-1}	3.74	3.38
temp, K	293 (2)	101 (2)
λ (Å)	0.710 73	0.909 00
R indicies [$I > 2\sigma(I)$][a]	R1 = 0.0930, wR2 = 0.1800	R1 = 0.0629, wR2 = 0.1880
R indicies (all data)[a]	R1 = 0.2363, wR2 = 0.3071	R1 = 0.0728, wR2 = 0.1975

[a] $R1 = \sum||F_o| - |F_c||/\sum|F_o|$; $wR2 = [\sum w(|F_o| - |F_c|)^2/\sum wF_o^2]^{1/2}$.

Table 2. Selected Interatomic Distances (Å) and Angles (deg) in [*cis*-Ti($\mu_{2,7}$-$OC_{10}H_6O$)$_2$$(py)_2$]$_n$ (**1**)

Ti−O1	1.841 (9)	Ti−N1	2.292 (11)	O2−C7	1.381 (14)
Ti−O2	1.939	Ti−N2	2.268 (10)	O3−C11	1.371 (14)
Ti−O3	1.853 (8)	O1−C1	1.356 (12)	O4−C15	1.373 (14)
Ti−O4	1.814 (8)				

O1−Ti−O3	100.4 (4)	N1−Ti−O1	85.9 (4)	N1−Ti−O4	84.7 (4)
O1−Ti−O2	93.9 (4)	N2−Ti−O1	169.4 (4)	N2−Ti−O4	84.3 (4)
O1−Ti−O4	95.8 (4)	N1−Ti−O3	173.7 (4)	N1−Ti−N2	83.6 (4)
O2−Ti−O3	94.8 (4)	N2−Ti−O3	90.1 (3)	Ti−O1−C1	152.8 (5)
O3−Ti−O4	95.4 (3)	N1−Ti−O2	83.8 (4)	Ti−O2−C7	138.6 (8)
O2−Ti−O4	164.4 (4)	N2−Ti−O2	83.8 (4)	Ti−O3−C11	143.0 (7)
				Ti−O4−C15	171.1 (8)

Results and Discussion

One-Dimensional Chain [*cis*-Ti($\mu_{2,7}$-$OC_{10}H_6O$)$_2$$py_2$]$_n$ (1). 1. Synthesis. Treatment of (^{i}PrO)$_4$Ti with 2,7-dihydroxynaphthalene in pyridine for 2 weeks at 100 °C afforded large orange crystals of the one-dimensional ladder [*cis*-Ti($\mu_{2,7}$-$OC_{10}H_6O$)$_2$-py_2]$_n$ (**1**):

$$(^iPrO)_4Ti + 2,7\text{-}HOC_{10}H_6OH \xrightarrow[100\ °C]{\text{pyridine}} \underset{\mathbf{1}}{[cis\text{-}Ti(\mu_{2,7}\text{-}OC_{10}H_6O)_2py_2]_n} + 4\ ^iPrOH \quad (1)$$

Inspection of the material by light microscopy revealed various-sized prisms, and the powder X-ray diffraction (XRD) pattern of the bulk matched that calculated from single-crystal diffraction studies, although a minor impurity phase was evident. A ^{1}H NMR spectrum of crystalline **1** degraded in CD_3OD/DCl revealed a 1:1 ratio of $DOC_{10}H_6OD$:py. From these observations **1** appears to be the major product of the reaction.

2. X-ray Crystal Structure of 1. Crystallographic information on data aquisition and refinement is given in Table 1, and pertinent bond distances and angles of [*cis*-Ti($\mu_{2,7}$-$OC_{10}H_6O$)$_2$-py_2]$_n$ (**1**) are listed in Table 2. Because of the weakly diffracting nature of the crystals, the 2σ data effectively gave a resolution of ∼1.3 Å (based on $\lambda/2 \sin\theta_{max}$) and the aromatic rings were restrained to be flat.

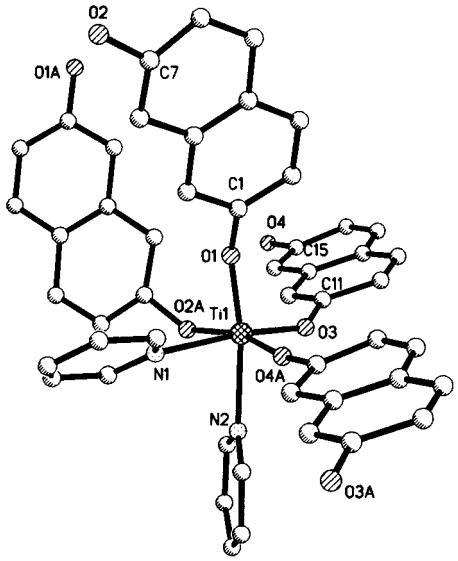

Figure 2. Subtly distorted *cis*-$(ArO)_4Tipy_2$ core of [*cis*-Ti($\mu_{2,7}$-OC10H6O)$_2$py$_2$]$_n$ (**1**).

Figure 2 illustrates the somewhat distorted *cis*-$(ArO)_4Tipy_2$ core of [*cis*-Ti($\mu_{2,7}$-$OC_{10}H_6O)_2py_2]_n$ (**1**), whose geometry is reminiscent of [*cis*-Ti($\mu_{1,4}$-$OC_6H_4O)_2py_2]_n$, which has a two-dimensional pleated sheet structure.[11,12] The pyridine ligands are constricted about the titanium as revealed by the N1−Ti−N2 angle of 83.6(4)°, while the *cis*-2,7-naphthalenedioxide ligands span 100.4(4)° (∠O1−Ti−O3). As a consequence the *cis*-O_{cis}−Ti−N angles are fairly normal (85.9(4)°, 90.1(3)°), but the *trans*-O_{cis}-Ti−N angles show some deviation from linearity (169.4(4)°, 173.7(4)°). The *trans*-2,7-naphthalenedioxides are canted (∠O2−Ti−O4 = 164.4(4)°) slightly away from their cis congeners ($\angle O_{trans}-Ti-O_{cis}$ = 95.0(8)°$_{ave}$) and toward the pyridines ($\angle O_{trans}-Ti-N$ = 84.2(4)°$_{ave}$).

While the angular distortions parallel those previously seen for this core, the core distances hold a singular surprise. The titanium−nitrogen (2.292(11), 2.268(10) Å) distances are normal, and the opposing titanium−oxygen bond lengths are somewhat short (1.841(9), 1.853(8) Å) in comparison to the average $d(Ti-O_{trans})$ of 1.877 Å, as expected from trans-influence arguments. However, the bond distances of the two *trans*-2,7-naphthalenedioxides are quite distinct, with d(Ti−O2) = 1.939(9) Å, significantly (∼4 × 3σ) longer than d(Ti−O4) = 1.814(8) Å. In addition, the longer bond has a corresponding ∠Ti−O2−C7 = 138.6(8)°, which is substantially more bent than that of the shorter bond (∠Ti−O4−C15 = 171.1(8)°). Although Rothwell has shown that the corollation between bond distance and bond angle in aryloxide coordination is tenuous at best,[17] in this instance the odd, long bond length may be a consequence of the contortion the O1,O2-naphthalenedioxide incurs in order to form the unusual triangularly spaced rungs of the zigzag one-dimensional ladder. Alternatively, the disparate trans Ti−O bond lengths may be a consequence of the trans influence of two strong-field ligands. A lesser difference in $d(Ti-O_{trans})$ is observed for [*cis*-Ti($\mu_{1,4}$-$OC_6H_4O)_2py_2]_n$[11,12] and the related two-dimensional complex below.

Figure 3 illustrates the zigzag-runged ladder structure of [*cis*-Ti($\mu_{2,7}$-$OC_{10}H_6O)_2py_2]_n$ (**1**) from perpendicular (Figure 3a) and parallel (Figure 3b) vantages. Bridging aryldioxides alternate above and below the plane of titaniums to connect in a triangular pattern and form the rungs. Likewise, the O3,O4-naphthalenedioxide linkages that comprise the sides are on opposite faces of the plane of titaniums, and the cis pyridines are oriented outward and inside the triangular cavities. The pyridine oriented to the inside the ladder interacts in an edge-to-face manner with one ring of a $\mu_{2,7}$-$OC_{10}H_6O$ bridge that comprises the adjacent rung (centroid to centroid d = 4.80 Å). In contrast, the externally oriented pyridine engages in a face-to-face π interaction with the middle inside portion of the $\mu_{2,7}$-$OC_{10}H_6O$ side of another ladder (pyridine centroid to naphthalene plane d = 3.88 Å). The edge of the external pyridine also interacts with the faces of $\mu_{2,7}$-$OC_{10}H_6O$ rungs of the neighboring zigzag-runged ladder. It is these π-stacking arrangements[18,19] that allow the ladders to interact and pack efficiently in the solid state.

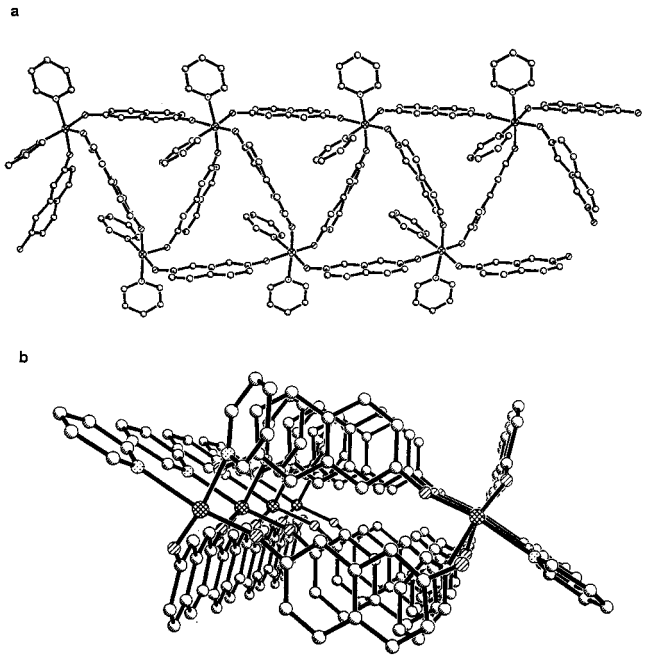

Figure 3. Perpendicular (a) and parallel (b) views of the zigzag-runged ladder structure of [*cis*-Ti($\mu_{2,7}$-OC10H6O)$_2$py$_2$]$_n$ (**1**).

Two-Dimensional [Ti($\mu_{2,7}$-$OC_{10}H_6O)_2$(4-picoline)$_2$·(4-picoline)$_{0.5}]_n$ (2). 1. Synthesis. To investigate the properties of an inorganic polymer of this type in solution, a more soluble derivative of [*cis*-Ti($\mu_{2,7}$-$OC_{10}H_6O)_2py_2]_n$ (**1**) was sought. Thermolysis of (^{i}PrO)$_4$Ti with 2,7-dihydroxynaphthalene in 4-methylpyridine at 100 °C generated crystals of [Ti($\mu_{2,7}$-$OC_{10}H_6O)_2$-(4-picoline)$_2$·(4-picoline)$_{0.5}]_n$ (**2**) after 2 days,

$$(^iPrO)_4Ti + 2,7\text{-}HOC_{10}H_6OH \xrightarrow[100\ °C]{\text{4-picoline}} 4\,^iPrOH + \underset{\mathbf{2}}{[Ti(\mu_{2,7}\text{-}OC_{10}H_6O)_2(4\text{-pic})_2\cdot(4\text{-pic})_{0.5}]_n} \quad (2)$$

and the red-orange flakes were harvested after 2 months. The powder XRD pattern of the bulk—after 2 weeks or 2 months—matched that calculated from single-crystal diffraction studies. The thin crystalline plates were small and required data collection at the Cornell High Energy Synchrotron Source (CHESS). A ^{1}H NMR spectrum of crystalline **2** degraded in CD_3OD/DCl revealed a $DOC_{10}H_6OD$/4-picoline ratio of 1:1.25, consistent with the stoichiometry of the crystals.

(17) Steffey, B. D.; Fanwick, P. E.; Rothwell, I. P. *Polyhedron* **1990**, *9*, 963−968.

(18) Mecozzi, S.; West, A. P.; Dougherty, D. A. *Proc. Natl. Acad. Sci. U.S.A.* **1996**, *93*, 10566−10571.

(19) (a) Klebe, G.; Diederich, F. *Philos. Trans. R. Soc. London A* **1993**, *345*, 37−48. (b) Bacon, G. E.; Curry, N. A.; Wilson, S. A. *Proc. R. Soc. London A* **1964**, *279*, 98−110.

Table 3. Selected Interatomic Distances (Å) and Angles (deg) in [*cis*-Ti($\mu_{2,7}$-$OC_{10}H_6O$)$_2$(4-Me-py)$_2$·(4-Me-py)$_{0.5}$]$_n$ (**2**)

Ti1−O1	1.846 (3)	Ti2−O8	1.850 (3)	O5−C21	1.339 (5)
Ti1−O3	1.852 (3)	Ti1−N1	2.298 (4)	O7−C31	1.346 (5)
Ti1−O5	1.875 (3)	Ti1−N2	2.287 (4)	O2−C5	1.358 (5)
Ti1−O7	1.859 (3)	Ti2−N3	2.303 (4)	O4−C17	1.355 (6)
Ti2−O2	1.871 (3)	Ti2−N4	2.294 (4)	O6−C27	1.355 (5)
Ti2−O4	1.861 (3)	O1−C1	1.351 (5)	O8−C35	1.353 (5)
Ti2−O6	1.847 (3)	O3−C11	1.362 (6)		
O1−Ti1−O3	94.63 (14)	N1−Ti1−O1	85.72 (14)	N4−Ti2−O2	86.83 (13)
O1−Ti1−O5	167.60 (15)	N1−Ti1−O3	89.88 (14)	N4−Ti2−O4	86.65 (15)
O1−Ti1−O7	95.05 (14)	N1−Ti1−O5	85.19 (14)	N4−Ti2−O6	83.70 (14)
O3−Ti1−O5	93.76 (13)	N1−Ti1−O7	168.90 (14)	N4−Ti2−O8	171.93 (15
O3−Ti1−O7	101.08 (14)	N2−Ti1−O1	83.90 (14)	Ti−O1−C1	161.4 (3)
O5−Ti1−O7	92.27 (14)	N2−Ti1−O3	172.37 (14)	Ti1−O3−C11	141.6 (3)
O2−Ti2−O4	92.10 (14)	N2−Ti1−O5	86.57 (13)	Ti1−O5−C21	147.3 (3)
O2−Ti2−O6	167.64 (15)	N2−Ti1−O7	86.51 (13)	Ti1−O7−C31	146.2 (3)
O2−Ti2−O8	93.79 (13)	N3−Ti2−O2	85.16 (14)	Ti2−O2−C5	147.3 (3)
O4−Ti2−O6	95.25 (14)	N3−Ti2−O4	168.94 (14)	Ti2−O4−C17	145.2 (3)
O4−Ti2−O8	101.37 (15)	N3−Ti2−O6	85.74 (14)	Ti2−O6−C27	161.3 (3)
O6−Ti2−O8	94.49 (14)	N3−Ti2−O8	89.52 (14)	Ti2−O8−C35	142.0 (3)

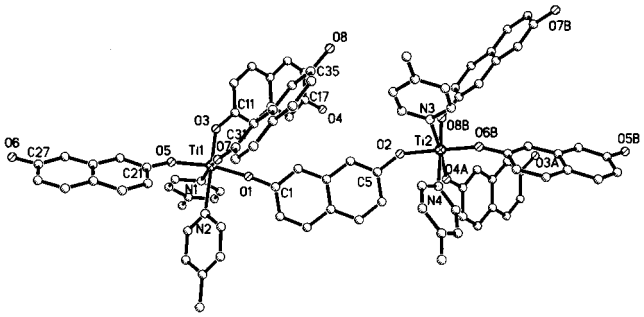

Figure 4. Crystallographically distinct *cis*-$(ArO)_4TiN_2$ cores of [Ti($\mu_{2,7}$-OC10H6O)$_2$(4-picoline)$_2$·(4-picoline)$_{0.5}$]$_n$ (**2**).

2. X-ray Crystal Structure of 2. Data collection and refinement information for [Ti($\mu_{2,7}$-$OC_{10}H_6O$)$_2$(4-picoline)$_2$·(4-picoline)$_{0.5}$]$_n$ (**2**) is listed in Table 1, and core bond distances and angles are given in Table 3. Note that **2** possesses two titanium cores per asymmetric unit, as illustrated in Figure 4; hence, the geometric parameters for both are listed. A brief perusal of Table 3 in comparison to the geometric parameters listed for [*cis*-Ti($\mu_{2,7}$-$OC_{10}H_6O$)$_2$py$_2$]$_n$ (**1**) in Table 2 reveals a virtual one-to-one correspondence for the features of each *cis*-$(ArO)_4TiN_2$ core. The comments above apply equally to **2** except that the disparity in *trans*-2,7-$OC_{10}H_6O$ distances is not so distinct (d(Ti1−O1) = 1.846(3) Å, d(Ti2−O6) = 1.847(3) Å vs d(Ti1−O5) = 1.875(3) Å, d(Ti2−O2) = 1.871(3) Å).

At first glance the two-dimensional, two-ply secondary structure of [*cis*-Ti($\mu_{2,7}$-$OC_{10}H_6O$)$_2$(4-picoline)$_2$·(4-picoline)$_{0.5}$]$_n$ (**2**) illustrated in Figure 5b appears vastly different from the zigzag-runged ladder of [*cis*-Ti($\mu_{2,7}$-$OC_{10}H_6O$)$_2$py$_2$]$_n$ (**1**). Two separate planes of titaniums are covalently linked via bridging 2,7-$OC_{10}H_6O$ units in the nominal fashion. As shown in Figure 5a, when a row of titanium cores from each layer of **2** is stripped of all additional connections, a ladder similar to that of **1** is revealed. Two externally oriented and two internally directed 4-picolines are evident, and the sides are composed of 2,7-$OC_{10}H_6O$ ligands with one short Ti−O bond accompanying a nearly linear Ti−O−C angle (∠Ti1−O1−C1 = 161.4(3)°, ∠Ti2−O6−C27 = 161.3(3)°) and one longer bond with a bent Ti−O−C angle (∠Ti1−O5−C21 = ∠Ti2−O2−C5 = 147.3-(3)°). When the middle of this ladder is compared to the zigzag rungs of **1**, it is obvious that every other rung is missing. Instead of connecting the sides, the O3,O4- and O7,O8-$\mu_{2,7}$-$OC_{10}H_6O$ bridges establish the covalent bonds with other ladders; thus, the two-ply motif can be visualized as a series of stacked ladders.

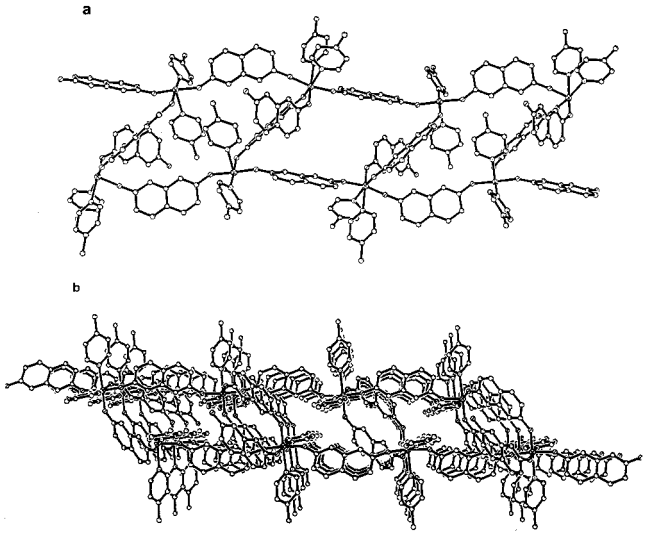

Figure 5. Missing rung ladder (a) of [Ti($\mu_{2,7}$-OC10H6O)$_2$(4-picoline)$_2$·(4-picoline)$_{0.5}$]$_n$ (**2**) that aggregates to the stacked ladder, two-ply, two-dimensional network (b).

In retrospect, the shift from a one-dimensional ladder to a different motif should have been expected when pyridine was replaced with 4-picoline. Recall that pyridine-face-to-2,7-naphthalenedioxide-face π-stacking interactions were critical to the packing of [*cis*-Ti($\mu_{2,7}$-$OC_{10}H_6O$)$_2$py$_2$]$_n$ (**1**). The simple replacement of an H by a Me on the pyridine disrupts this packing by rendering the interpenetration of the ladders implausible. Second, the internal pyridine edge to naphthalene ring interaction evident in **1** is impossible with a Me group in the 4-position of the pyridine ring. No significant π interactions,[18,19] either edge-to-face or face-to-face, have been observed in [*cis*-Ti($\mu_{2,7}$-$OC_{10}H_6O$)$_2$(4-picoline)$_2$·(4-picoline)$_{0.5}$]$_n$ (**2**). The covalent linkages binding the stacked ladders of **2** must help compensate for the lost π interactions of **1**, although the total number of titanium−aryloxide bonds is the same in both structures. It is possible that the intermolecular arrangement in **2** is less strained than the zigzag binding of the $\mu_{2,7}$-$OC_{10}H_6O$ groups in **1**, at least from the standpoint of bond lengths and angles. In turn, the intramolecular π interactions in **1** keep it from reverting to the double sheet, stacked ladder motif of **2**. These interpretations must be assessed with care because despite the rather lengthy time both compounds underwent thermolysis, it cannot be certain that the structure types elicited for each

Table 4. Polyethylene data from CMON and Related Compounds with MAO[a] (Eq 3)

catalyst	D (g/cm^3)	activity[b]	mp (°C)[c]	Mn[d]	MW[d]	MW/Mn[d]
amorphous		0.4	116			
Ti prepowder						
zero-dimensional						
[Ti)OPh)$_3$(HOPh)]$_2$(μ-OPh)$_2$[e,f]	1.310	25.6	122	2300	303 000	129
one-dimensional						
[*cis*-Ti($\mu_{2,7}$-OC$_{10}$H$_6$O)$_2$py$_2$]$_n$ (**1**)	1.361	27.6	122			
two-dimensional						
[*trans*-Ti($\mu_{1,4}$-OC$_6$H$_4$-O)$_2$py$_2$·py]$_n$[g]	1.357	15.3	121	1100	116 000	104
[*trans*-Ti($\mu_{1,4}$-OC$_6$H$_4$O)$_2$(4-Ph-py)$_2$]$_n$[g]	1.411	14.3	120		274 000	107
[*cis*-Ti($\mu_{2,7}$-OC$_{10}$H$_6$O)$_2$(4-picoline)$_2$·(4-picoline)$_{0.5}$]$_n$ (**2**)	1.364	12.3	121	2600		
[*trans*-Ti($\mu_{1,3}$-OC$_6$H$_4$O)$_2$py$_2$]$_n$[g]	1.480	9.0	122			
[*cis*-Ti($\mu_{1,4}$-OC$_6$H$_4$O)$_2$py$_2$]$_n$[g,h]	1.406	5.5	120			
[*trans*-Ti($\mu_{1,3}$-OC$_6$H$_4$O)$_2$(4-Ph-py)$_2$]$_n$[g]	1.390	3.6	119			
{[Ti($\mu_{1,3}$-1,3-OC$_6$H$_4$O)(μ-1,3-OC$_6$H$_4$OH) (1,3-OC$_6$H$_4$OH)(HO^{i}Pr)]$_2$}2}$_n$[i]	1.453	0.9	117			
three-dimensional						
{[Ti(μ:η^2,η^1-4,4′-OC$_{12}$H$_8$O)$_{0.5}$(μ-4,4′-OC$_{12}$H$_8$O)(O^{i}Pr)(HO^{i}Pr)]$_2$·THF}$_n$[i]	1.310	9.9	122			
[Ti$_2$($\mu_{2,7}$-OC$_{10}$H$_6$O)$_2$($\mu_{2,7}$:η^2,η^1-OC$_{10}$H$_6$OH)$_2$(O^{i}Pr)$_2$]$_n$[j]	1.451	0.5	121			
[Ti$_2$($\mu_{1,4}$-OC$_6$H$_4$O)$_2$($\mu_{1,4}$:η^2,η^1-OC$_6$H$_4$O)$_2$(OH$_2$)$_2$·(H$_2$O)$_2$·(HOC$_6$H$_4$OH)·(MeCN)]$_n$[j]	1.518	0.5	118			
[Ti$_2$($\mu_{1,4}$-OC$_6$H$_4$O)$_2$($\mu_{1,4}$-OC$_6$H$_4$OH)$_2$(μ-OC$_6$H$_4$OH)$_2$]$_n$[h,j]	1.535	0.2	120	3100	717 000	233

[a] Al/Ti = 1000:1. [b] g PE/(mmol Ti h). [c] Onset temperature by DSC. All transitions were sharp with a peak temperature of 132 °C. [d] GPC in 1,2,4-trichlorobenzene at 135 °C. [e] Al/Ti = 1046:1. [f] Reference 20. [g] Reference 14. [h] Reference 11. [i] Reference 13. [j] Reference 12.

Table 5. Polypropylene Data from CMON and Related Compounds with MAO[a] (Eq 3)

catalyst	activity[b]	Mn[c]	MW[c]	MW/Mn[c]
amorphous				
Ti prepowder[d]	0.0			
zero-dimensional				
[Ti(OPh)$_3$(HOPh)]$_2$(μ-OPh)$_2$[e]	2.6	24000	19 0000	8
one-dimensional				
[*cis*-Ti($\mu_{2,7}$-OC$_{10}$H$_6$O)$_2$py$_2$]$_n$ (**1**)	1.0	3200	27 000	8
two-dimensional				
[*trans*-Ti($\mu_{1,4}$-OC$_6$H$_4$−O)$_2$py$_2$·py]$_n$[f]	0.3	3500	33 000	9.5
[*trans*-Ti($\mu_{1,4}$-OC$_6$H$_4$O)$_2$(4-Ph-py)$_2$]$_n$[f]	0.0			
[*cis*-Ti($\mu_{2,7}$-OC$_{10}$H$_6$O)$_2$(4-picoline)$_2$·(4-picoline)$_{0.5}$]$_n$ (**2**)	0.5			
[*trans*-Ti($\mu_{1,3}$-OC$_6$H$_4$O)$_2$py$_2$]$_n$[f]	0.2			
[*cis*-Ti($\mu_{1,4}$-OC$_6$H$_4$O)$_2$py$_2$]$_n$[f,g]	1.0	5500	10 000	1.8
[*trans*-Ti($\mu_{1,3}$-OC$_6$H$_4$O)$_2$(4-Ph-py)$_2$]$_n$[f]	0.1			
{[Ti($\mu_{1,3}$-1,3-OC$_6$H$_4$O)(μ-1,3-OC$_6$H$_4$OH)(1,3-OC$_6$H$_4$OH)(HO^{i}Pr)]$_2$}$_n$[h]	0.0			
three-dimensional				
{[Ti(μ:η^2,η^1-4,4′-OC$_{12}$H$_8$O)$_{0.5}$(μ-4,4′-OC$_{12}$H$_8$O)(O^{i}Pr)(HO^{i}Pr)]$_2$·THF}$_n$[h]	1.4	1600	22 000	8
[Ti$_2$($\mu_{2,7}$-OC$_{10}$H$_6$O)$_2$($\mu_{2,7}$:η^2,η^1-OC$_{10}$H$_6$OH)$_2$(O^{i}Pr)$_2$]$_n$[i]	0.0			
[Ti$_2$($\mu_{1,4}$-OC$_6$H$_4$O)$_2$($\mu_{1,4}$:η^2,η^1-OC$_6$H$_4$O)$_2$(OH$_2$)$_2$·(H$_2$O)$_2$·(HOC$_6$H$_4$OH)·(MeCN)]$_n$[i,j]	0.0			
[Ti$_2$($\mu_{1,4}$-OC$_6$H$_4$O)$_2$($\mu_{1,4}$-OC$_6$H$_4$OH)$_2$(μ-OC$_6$H$_4$OH)$_2$]$_n$[g,i]	0.0			

[a] Al/Ti = 1000:1 unless otherwise noted. [b] g PE/(mmol Ti h). [c] GPC in THF at 23 °C. [d] Al/Ti = 1048:1. [e] Reference 20. [f] Reference 14. [g] Reference 11. [h] Reference 13. [i] Reference 12. [j] Al/Ti = 782:1.

represent the thermodynamic products of their respective systems.

CMON Polymerization Studies. Including the compounds above, representative one-, two- and three-dimensional titanium CMON materials have been synthesized and characterized by X-ray diffraction studies. This set of CMON, augmented by the "zero-dimensional" control complex [Ti(OPh)$_3$(HOPh)]$_2$(μ-OPh)$_2$[20] and an amorphous oligomer formed from (^{i}PrO)$_4$Ti and hydroquinone ([Ti(OC$_6$H$_4$O)$_a$(O−C$_6$H$_4$OH)$_{3.34-1.83a}$(O^{i}Pr)$_{0.66-0.17a}$-(THF)$_{0.2}$]$_n$),[12] was amenable to screening for polymerization activity in the presence of cocatalyst methylaluminoxane (MAO) according to the equation

$$H_2C{=}CHR\ (5.4\ atm) \xrightarrow[23\ °C,\ 2\ h]{CMON/MAO\ (excess)} polyolefin \quad (3)$$

Each CMON compound (∼4 mg) was slurried in toluene, and activated with a vast excess of MAO at 23 °C under ∼5 atm of ethylene or propylene for 2 h. Each run was then quenched with cold methanol, and the residual catalyst and aluminum products were dissolved in aqueous HCl and separated. Evaporation of the toluene typically left 3−500 mg of polymer, depending on the catalyst. The results for ethylene are given in Table 4 and those for propylene in Table 5.

The ethylene polymerization activity of the titanium CMON was mediocre to poor, ranging from 28 to 0.2 g PE/(mmol Ti h) (Table 4). Furthermore, difficulties in analyzing the relatively high melting polyethylene curtailed examination of all but a few of the catalyst runs. The polyethylene obtained was a spongy, white, variable molecular weight polymer whose insolubility made it difficult to obtain molecular weight data, although several samples were eventually analyzed by gel permeation chromatography (GPC) in 1,2,4-trichlorobenzene at 135 °C. Melting points were relatively invariant of the catalyst used, the onset temperatures determined by differential scanning calorimetry (DSC) varied from 116 to 122 °C, and a relatively sharp transition was observed with a peak temperature of 132 °C. These data are fully consistent with a linear material.[21] Although it is tempting to conclude that [Ti$_2$($\mu_{1,4}$-OC$_6$H$_4$O)$_2$-($\mu_{1,4}$-OC$_6$H$_4$OH)$_2$(μ-OC$_6$H$_4$OH)$_2$]$_n$ is superior to the other catalysts on a molecular weight basis, it is equally plausible

(20) (a) Svetich, G. W.; Voge, A. A. *J. Chem. Soc., Chem. Commun.* **1971**, 676−677. (b) Svetich, G. W.; Voge, A. A. *Acta Crystallogr.* **1972**, *B28*, 1760−1767.

that the numbers reflect the inability to obtain data that are truly representative of the entire sample. For example, with both polyethylene and polypropylene some insoluble polymer was retained on the filter of the GPC injection syringe. All of the polydispersity indexes (PDI's) listed are extremely high (104−233), and any loss of either high- or low-end molecular weight material can skew the numbers significantly. With these caveats in mind, it is likely that similar distributions of polymer chain length are obtained for each CMON catalyst under the standard conditions employed.

Fortunately, a reasonably diverse group of samples were analyzed and some general conclusions regarding the efficacy of CMON catalysts can be made. The best catalysts, from the standpoint of activity, were the molecular complex, $[Ti(OPh)_3(HOPh)]_2(\mu\text{-}OPh)_2$,[20] and $[cis\text{-}Ti(\mu_{2,7}\text{-}OC_{10}H_6O)_2py_2]_n$ (**1**), the lone one-dimensional representative. These are followed by several two-dimensional derivatives whose structures consist of sheets held together via the interpenetration and π interactions of pyridine-based ligands[14] and $[Ti(\mu_{2,7}\text{-}OC_{10}H_6O)_2(4\text{-picoline})_2\cdot(4\text{-picoline})_{0.5}]_n$ (**2**). Finally, a single three-dimensional material, $\{[Ti(4,4'\text{-}OC_{12}H_8O)_{1.5}(O^iPr)(HO^iPr)]_2\cdot THF\}_n$, which possesses a primitive secondary structural motif, has an activity (9.9 g PE/(mmol Ti h)) that approaches the good two-dimensional materials. The amorphous precursor material $[Ti(OC_6H_4O)_a(OC_6H_4OH)_{3.34-1.83a}(O^iPr)_{0.66-0.17a}(THF)_{0.2}]_n$ [12] proved to be a surprisingly poor catalyst, perhaps suggesting that it is sufficiently cross-linked to be considered a relatively dense three-dimensional material. Others have used amorphous titanium and zirconium aryloxide polymers as Lewis acid catalysts, for instance, in the Diels−Alder condensation of acrolein and 1,3-cyclohexadiene.[22,23] Perhaps well-defined crystalline compounds would have even better Lewis acid catalytic activity by analogy.

The propylene polymerization activity (0.0−2.6 g PP/(mmol Ti h)) was substantially worse than the polyethylene runs, with only a few catalysts truly operative. The polypropylene obtained was a sticky, elastic, atactic polymer, and DSC performed on a representative sample showed no melting point transition, while ^{13}C NMR (CD_2Cl_2) spectral analyses[24] of several samples indicated that the polymer was atactic. A few runs generated enough polypropylene to merit analysis by GPC at 23 °C, and the molecular weights are given in Table 5. The CMON yielded material whose molecular weights were substantially lower than that from the polyethylene runs and possessed PDI's that were correspondingly lower. While differing solubilities of polyethylene and polypropylene and the different analytical solvent systems employed may contribute to the disparities in molecular weight, these differences in reactivity of ethylene vs propylene are rather typical of Ziegler−Natta systems.

For the polyethylene results, a rough inverse dependence on dimensionality of the CMON catalyst is apparent, although exceptions persist within each group. The "zero" and one-dimensional materials are best, followed by some of the two-dimensional materials. It is difficult to understand why some of the 2-D CMON are moderately effective, while others are not, but speculation suggests that structural features other than dimensionality may be important. Two of the 2-D CMON that are active are of relatively low density ($[trans\text{-}Ti(\mu_{1,4}\text{-}OC_6H_4O)_2py_2\cdot py]_n$, $D = 1.357$ g/cm^3 (Figure 1); $[cis\text{-}Ti(\mu_{2,7}\text{-}OC_{10}H_6O)_2(4\text{-picoline})_2\cdot(4\text{-picoline})_{0.5}]_n$ (**2**), $D = 1.364$ g/cm^3) in comparison to the remainder. While the low density of **2** is in part due to its greater light atom to Ti ratio intrinsic to the longer spacer and substituted pyridine, both compounds have intercalated molecules that can be lost during MAO/monomer initiation and both have relatively large channels that can aid in lattice degradation and activation, etc. Activation of the networks must occur initially at the surface, but the ease with which the network can be degraded to enable new catalytic centers must be critical. Note that the best three-dimensional catalyst, $\{[Ti(\mu\text{:}\eta^2,\eta^1\text{-}4,4'\text{-}OC_{12}H_8O)_{0.5}(\mu\text{-}4,4'\text{-}OC_{12}H_8O)(O^iPr)(HO^iPr)]_2\cdot THF\}_n$ (Figure 1) is the least dense of its class. It has a primitive connectivity rather than the body-centered or hexagonal motifs of its congeners, and it has larger channels.

Functionality must also play a role in tempering activation and reactivity. All of the surfaces of the CMON crystallites are terminated with hydroxyls, and these would presumably need to be quenched by the Al−Me groups of MAO before activation of the titaniums could be initiated. In view of such phenomena associated with the size of the catalyst particles, care was taken to grind each material to a similar size, but such procedures provide rough uniformity at best, and under slurry conditions, some materials would undoubtedly fracture more readily than others. The 2-D materials have "dangling hydroxyl" groups only at the edges and not the surfaces of the sheets, and $[cis\text{-}Ti(\mu_{2,7}\text{-}OC_{10}H_6O)_2py_2]_n$ (**1**) has such functionality only at the ends of the chains. In contrast, crystallites of the 3-D CMON have surfaces that are essentially completely hydroxylated, requiring greater quenching by MAO. These arguments assume that a lower "effective Al/Ti ratio" would lessen the activity of the catalyst, but it is possible that such surface functionality could aid in the destruction of the lattice and help access more titanium sites. Because of the observations concerning activity that is roughly inversely dependent on dimensionality, the latter conjecture does not appear correct. Note that two-dimensional $\{[Ti(\mu_{1,3}\text{-}1,3\text{-}OC_6H_4O)(\mu\text{-}1,3\text{-}OC_6H_4OH)(1,3\text{-}OC_6H_4OH)(HO^iPr)]_2\}_n$ (0.9 g PE/(mmol Ti h)), whose layers are essentially hydroxylated on both faces, is the poorest catalyst of this class of CMON. It had been expected that the loss of pyridine or like ligands during the course of activation and reaction might quench certain catalyst sites, but this was not observed.

As each ethylene polymerization proceeded, particles were no longer visible and the solutions took on the same orange coloration, despite the different catalysts employed. In nonliving chain polymerization processes[25] typical of Ziegler−Natta systems, propagation rates are usually exceedingly fast, and the efficacy of initiation should not impact the polydispersity. While it was hoped that degradation of certain CMON materials would occur in a more uniform fashion, the broad distributions of polyethylene and polypropylene generated via CMON catalysts are best considered indicative of numerous active sites having differing rates of propagation, chain transfer, and termination. It is likely that fragmentation of the CMON lattices occurs spuriously, generating several active sites in various stages of aggregation and ligation.

Conclusions

In the exploration of the scope of covalent metal−organic networks (CMON), larger organic spacers were employed. In

(21) *Concise Encyclopedia of Polymer Science and Engineering*; Kroschwitz, J. I., Ed.; Wiley-Interscience: New York, 1990.
(22) Sawaki, T.; Aoyama, Y. *J. Am. Chem. Soc.* **1999**, *121*, 4793−4798.
(23) For related molecular catalysis, see the following (and references therein). (a) Ishitani, H.; Yamashita, Y.; Kobayashi, S. *J. Am. Chem. Soc.* **2000**, *122*, 5403−5404. (b) Ishitani, H.; Komiyama, S.; Hasegawa, Y.; Kobayashi, S. *J. Am. Chem. Soc.* **2000**, *122*, 762−766. (c) Kobayashi, S.; Komiyama, S.; Ishitani, H. *Angew. Chem., Int. Ed.* **1998**, *37*, 979−981.
(24) Zambelli, A.; Locatelli, P.; Baho, G.; Bovey, F. A. *Macromolecules* **1975**, *8*, 687−689.
(25) Misra, G. S. *Introductory Polymer Chemistry*; John Wiley & Sons: New York, 1993.

the case of 2,7-dihydroxynaphthalene and $(^{i}PrO)_4Ti$ in pyridine—a combination utilized in anticipation of forming large-channel two-dimensional CMON—the one-dimensional zigzag-runged ladder $[cis\text{-}Ti(\mu_{2,7}\text{-}OC_{10}H_6O)_2py_2]_n$ (**1**) was produced when a diagonal connectivity of $\mu_{2,7}\text{-}OC_{10}H_6O$ bridges was found to link together strands of $cis\text{-}(ArO)_4Tipy_2$ centers. Intraladder edge-to-face and interladder face-to-face π interactions of aromatic residues play critical structural roles that are interrupted when pyridine is replaced by 4-picoline. In 4-picoline, alternate "rungs" of the zigzag connections are broken and the ladders are covalently linked to produce two-dimensional $[cis\text{-}Ti(\mu_{2,7}\text{-}OC_{10}H_6O)_2(4\text{-picoline})_2\cdot(4\text{-picoline})_{0.5}]_n$ (**2**), which consists of stacked ladders. The subtle substitution of a methyl for a hydrogen on the pyridine ring results in a change in dimensionality of the coordination polymer brought about by a disruption of the π interactions found in **1**.

The discovery of the one-dimensional compound $[cis\text{-}Ti(\mu_{2,7}\text{-}OC_{10}H_6O)_2py_2]_n$ (**1**) provided an opportunity to complete an assay of titanium-based CMON in Ziegler−Natta polymerizations in the hope of finding a heterogeneous analogue to a single-site catalyst. Although a conceptually interesting approach, the catalysts displayed mediocre activity that was roughly inversely dependent on dimensionality of the network. The polyethylene obtained was polydisperse, although its melting points were within a relatively narrow range indicative of linear material. The data were consistent with catalyst degradation leading to numerous sites of variable activity. Under the conditions employed the CMON are relatively ineffective Ziegler−Natta catalysts because of the nonuniform degradation of each material; therefore, reactions that do not require CMON decomposition may be more suitable to be investigated from the standpoint of potential catalysis. Alternatively, organometallic features may be built into the CMON in order to more closely resemble homogeneous catalysts. The current CMON compounds might also be used as support materials in Ziegler−Natta or related systems, given the surface hydroxyl functionality present.

Experimental Section

General Considerations. All manipulations were performed on a high-vacuum line or in an inert atmosphere drybox unless otherwise noted. Tetrahydrofuran was distilled from purple sodium benzophenone ketyl and vacuum-transferred from the same into a glass bomb immediately prior to use in the drybox. Pyridine and 4-picoline were refluxed over sodium, subsequently vacuum-transferred onto activated 4 Å molecular sieves, and vacuum-transferred into a glass bomb for storage in the drybox. 2,7-Dihydroxynaphthalene (Aldrich, 97%) was dried by dissolving in dry THF and then removing the volatiles; this procedure was repeated three times. $(^{i}PrO)_4Ti$ (Aldrich, 97%) was used as received and stored in the drybox. DCl (20 wt % in D_2O, Aldrich) and CD_3OD (Cambridge Isotope Laboratories, D, 99.8%) were used as received; solutions for ^1H NMR spectroscopy were ca. 3 wt % DCl (∼1 M) and were prepared on the benchtop. Methylaluminoxane (7.1 wt % Al in toluene) was purchased from AKZO-Nobel Chemicals and stored in the glovebox. Ethylene (99.6%) and propylene (99%) were purchased from Matheson.

^1H NMR spectra were obtained on a Varian XL-200 spectrometer. Powder diffraction was performed on a Scintag XRD system-interfaced PC with Windows NT. Standard powder patterns were recorded as continuous scans with a chopper increment of 0.03° 2θ and a scan rate of 2° per minute.

Procedures. 1. Preparation of $[cis\text{-}Ti(\mu_{2,7}\text{-}OC_{10}H_6O)_2py_2]_n$ (1). $(^{i}PrO)_4Ti$ (300 mg, 1.06 mmol) was added to a suspension of 2,7-dihydroxynaphthalene (338 mg, 2.1 mmol) and pyridine (∼3 mL) in a glass tube to give an orange solution and precipitate. The tube was sealed under vacuum and heated at 100 °C for 2 weeks, resulting in large orange crystals that were collected by filtration, washed with THF, and dried in vacuo for ∼10 min. Inspection of a sample in Paratone oil under a microscope revealed the crystals to be orange prisms of various sizes. Powder XRD matched the theoretical pattern obtained from single-crystal diffraction studies, although a minor phase was also evident. A ^1H NMR spectrum of a sample degraded in CD_3OD/DCl indicated a 1:1 ratio of $DOC_{10}H_6OD$/py. Anal. Calcd for $C_{30}H_{22}O_4N_2Ti$ (found): C, 69.00 (68.79); H, 4.22 (4.23); N, 5.37 (5.28). IR (Nujol, cm^{-1}): 1612(s), 1586(s), 1248(s), 1209(s), 1145(s), 1067(m), 1042(m), 1011(m), 983(w), 955(s), 851(s, br), 824(s), 779(m), 760(s), 695(s), 653(w), 634(s), 614(w), 575(s), 556(s), 539(s), 494(m), 469(w), 441(m), 430(m).

2. Preparation of $[Ti(\mu_{2,7}\text{-}OC_{10}H_6O)_2(4\text{-picoline})_2.(4\text{-picoline})_{0.5}]_n$ (2). $(^{i}PrO)_4Ti$ (300 mg, 1.06 mmol) was added to a suspension of 2,7-dihydroxynaphthalene (338 mg, 2.1 mmol) and 4-picoline (∼3 mL) in a glass tube to give a yellowish slurry. The tube was sealed under vacuum and heated at 100 °C for 2 months, even though crystals were evident after 2 days. The resulting crystals were collected by filtration, washed with THF on the benchtop, and immediately dried in vacuo for ∼10 min. Inspection of a sample in Paratone oil under a microscope revealed the crystals to be red-orange flakes of various shapes. Powder XRD matched the theoretical pattern obtained from single-crystal structure determination. A ^1H NMR spectrum of a sample quenched in CD_3OD/DCl indicated a 1:1.25 ratio of $DOC_{10}H_6OD$/4-picoline. Anal. Calcd for $C_{35}H_{29.5}O_4N_{2.5}Ti$ (found): C, 70.44 (69.60); H, 4.94 (4.98); N, 5.87 (5.74). IR (Nujol, cm^{-1}): 1725(w), 1680(w), 1246(s), 1209(s), 1146(s), 1112(m), 1067(w), 1017(m), 951(m), 859(s), 835(m), 801(m), 770(m), 725(w), 635(m), 583(m), 567(s), 504(w), 470(w), 451(m).

Polymerization Studies. In the glovebox, each finely ground catalyst (4 mg) was placed in a 3 ounce Fisher-Porter bottle apparatus (Andrews Glass Company) with a stir bar and enough toluene to make the total volume ∼10 mL once the MAO was added. The vessel was fitted with an O-ring and screw on coupling. The coupling was previously connected to a homemade Swagelok apparatus consisting of a pressure gauge, emergency pressure release valve, a Quik connect valve and another two-way valve. The Swagelok cap on the second valve had a GC septum inserted for the injection of the MAO. In a hood, the setup was purged with monomer around the GC septum and held with a slight pressure as the MAO was added. Methylaluminoxane (7.1 wt % Al in toluene) was measured with a 10 mL Gas-Tite syringe in the glovebox. The Al/Ti ratio was 1000:1 except as noted in Tables 4 and 5. The MAO was injected into the reaction vessel through the GC septum immediately upon removal from the glovebox, and the valve was closed for the duration of the run. The ethylene pressure was held at 80 psi (5.4 atm) for 2 h while the mixture was stirred at room temperature. The mixture was quenched with cold methanol, and the residual catalyst and aluminum products were dissolved by adding 1 M HCl. Evaporation of the toluene left the polymer, which was dried in air before being weighed.

X-ray Crystallographic Studies. 1. $[cis\text{-}Ti(\mu_{2,7}\text{-}OC_{10}H_6O)_2py_2]_n$ (1). Crystals large enough for structure determination were grown from pyridine as explained above. A few milligrams of crystals were suspended in Paratone oil on a glass slide. Under a microscope, a single red-orange prism (110 μm × 75 μm × 60 μm) was epoxied to a 1 mm length of glass wool that was previously attached to a thin glass fiber. X-ray diffraction data (1.79−20.90°; 8940 reflections, 2678 independent) were collected on a Siemens SMART system at 293 K. Observed intensities were corrected for Lorentz and polarization effects, and a semiempirical absorption correction was applied (SADABS). The structure was solved by direct methods (SHELXTL). Hydrogen atoms were added geometrically. Because of the weakly diffracting crystals of **1**, it was necessary to restrain the aromatic rings to be flat during the refinement (data/restraints/parameters = 1223/24/154) and the data were cut at a resolution of ∼1.3 Å (∼16°) in the final run. The structure was refined by full-matrix least-squares on F^2 using isotropic thermal parameters for all non-hydrogen atoms except titanium, which was refined anisotropically. The largest difference peak and hole were 0.335 and −0.264 e $Å^{-3}$, respectively.

2. $[Ti(\mu_{2,7}\text{-}OC_{10}H_6O)_2(4\text{-picoline})_2\cdot(4\text{-picoline})_{0.5}]_n$ (2). Crystals of **2** were grown from 4-picoline as explained above. A few milligrams of orange microcrystals were suspended in Paratone oil on a glass slide. Under a microscope, a single flat, orange chip (90 μm × 90 μm × 15

μm) was isolated in a rayon fiber loop epoxied to a metal fiber.[26,27] On the A1 line at CHESS, the crystal was frozen in a 101 K nitrogen stream. By use of a 0.1 mm collimator, a Quantum 4 CCD was used to record diffraction.[28] Data were collected for 45 s with 15 oscillations in φ, with a total of 360° collected. Observed intensities were corrected for Lorentz and polarization effects, and no absorption correction was applied. The first frame was indexed to a triclinic unit cell using the program DENZO,[29] and all the data (4.21−23.25°; 19 034 reflections) were scaled together with SCALEPACK (5658 unique reflections). The structure was solved by direct methods (SHELXTL) in $P1$, and after some initial refinement it was transferred into $P\bar{1}$. All hydrogen atoms were introduced geometrically. The structure was refined by full-matrix least-squares on F^2 using anisotropic thermal parameters for all non-hydrogen atoms. The largest difference peak and hole were 0.361 and −0.446 e Å^{-3}, respectively.

Acknowledgment. We thank John M. Pette and Emil B. Lobkovsky for experimental assistance and gratefully acknowledge contributions from the National Science Foundation (Grant CHE-9816134), the Cornell High Energy Synchrotron Source (CHESS), the Cornell Center for Materials Research (Grant DMR-9632275; Grant MSC REU to J.P.), and Cornell University.

Supporting Information Available: X-ray crystallographic files in CIF format for the structure determinations of *cis*-Ti($\mu_{2,7}$-$OC_{10}H_6O)_2$-$py_2]_n$ (**1**) and [Ti($\mu_{2,7}$-$OC_{10}H_6O)_2$(4-picoline)$_2$·(4-picoline)$_{0.5}]_n$ (**2**). This material is available free of charge via the Internet at http://pubs.acs.org.

IC000763N

(26) Blond, L.; Pares, S.; Kahn, R. *J. Appl. Crystallogr.* **1995**, *28*, 653−654.

(27) A thorough explanation of the construction of fiber loops and experimental methods at CHESS is given in the following. Walter, R. L. Ph.D. Thesis, Cornell University, Ithaca, NY, 1996.

(28) (a) Thiel, D. J.; Walter, R. L.; Ealick, S. E.; Bilderback, D. H.; Tate, M. W.; Gruner, S. M.; Eikenberry, E. F. *Rev. Sci. Instrum.* **1995**, *3*, 835−844. (b) Walter, R. L.; Thiel, D. J.; Barna, S. L.; Tate, M. W.; Wall, M. E.; Eikenberry, E. F.; Gruner, S. M.; Ealick, S. E. *Structure* **1995**, *3*, 835−844.

(29) Otwinski, Z. *DENZO, a program for automatic evaluation of film densities*; Department for Molecular Biophysics and Biochemistry, Yale University: New Haven, CT, 1988.